A Study of Delay and Doppler Spreads at 24 GHz ISM band

Smruti Ranjan Panigrahi*†, Shaikh Masud Rana*, Niclas Björsell* and Mats Bengtsson†
*Department of Electronics, Mathematics and Natural Sciences, University of Gävle, Sweden
†School of Electrical Engineering and Computer Science, KTH Royal Institute of Technology, Sweden
smruti.panigrahi@hig.se, shaikhmasudrana556677@gmail.com, niclas.bjorsell@hig.se, mats.bengtsson@ee.kth.se

***Abstract*—This article investigates the wide-band channel characteristics at 24 GHz ISM band in a mobile radio environment. The mobility in the test environment is achieved by attaching the transmit antenna to a KUKA robot's arm. The radio measurements were carried out inside the robotics lab at the University of Gävle, Sweden. The radio channel measurements were carried out at various situations, e.g., line of sight (LOS), non-line of sight (NLOS), regular lab environment, reflective environment, and different velocities of the robot's arm. The influence of these situations on the power delay profile, Doppler spectral density, root mean square (RMS) delay spread, RMS Doppler spread, coherence bandwidth and coherence time, has been studied.**

***Index Terms*—mmWave, power delay profile, Doppler spectral density, RMS Delay Spread, RMS Doppler Spread**

I. Introduction

The fifth-generation (5G) mobile communication is a paradigm shift in wireless technologies. It not only advances the mobile broadband services further, but also introduces lots of new use cases in the domain of internet of things (IoT), industrial internet of things (IIoT), and vehicular communication [1]. Millimeter-wave (mmWave) frequency bands, ranging from 24 GHz to 100 GHz, are one of the key features of 5G. Large available bandwidth, low interference and compact radio design are some of the benefits brought by the mmWave wireless technology. Therefore, it is necessary to measure and investigate the radio channel characteristics, in order to understand the challenges that likely arise from the propagation environments.

Radio channel measurements in the mmWave frequency bands were initially carried out in 1988 in an urban environment [2]. However, after the advent of 5G, the usage of mmWave frequency band for wireless communication has received more and more attention in recent years. In the last few years, several real-world measurements were carried out at 28, 38, 60 and 73 GHz in urban environments [3], [4] and indoor office environments [5], [6]. Some of the key channel characteristics addressed are path loss models, delay spread, number of multi-path components, outage probabilities, and spatial characteristics. Additionally, there were several measurements, and similar investigations performed at 26 GHz [7], 29 GHz [8], 60 GHz [9], [10], 61 GHz [11], and 83.5 GHz [12] for both LOS and NLOS situations in an indoor office environment. However, after a thorough literature review, we did not find any work, which investigates the Doppler effect on a real-world situation in any of the mmWave frequency band.

Moreover, we did not find any measurement activities performed at the 24 GHz frequency band. The radio measurement activities at 24 GHz are equally important as the frequency range from 24 to 24.25 GHz is reserved for industrial, scientific and medical (ISM) applications. During the previous generation of mobile technologies, ISM frequency bands are predominantly used in industrial wireless networking, home automation and broadband solutions, and IoT applications.

In this research article, we carried out the radio channel measurements by our in-house assembled low-cost testbed at 24 GHz frequency band. Additionally, the transmit antenna was attached to the arm of a Keller und Knappich Augsburg (KUKA) robot, in order to create motion in the measurement environment. KUKA is a German manufacturer of industrial robots and solutions for factory automation. The robotics lab at the University of Gävle, Sweden, was chosen for the measurements. The radio channel measurements were carried out at various situations, e.g., line of sight (LOS), non-line of sight (NLOS), regular lab environment, reflective environment, and two different velocities of robot's arm. In this article, we investigate the multi-path components and the Doppler effect. These channel effects are quantified by several wide-band channel parameters, like RMS delay spread, RMS Doppler spread, coherence bandwidth and coherence time.

The rest of this paper is organized as follows. Section II describes the measurement methodology. Section III presents the theoretical aspects of the wide-band channel characterization to understand the analysis of the results. Measurement results are analyzed in Section IV. Section V concludes the paper.

II. Measurement Methodology

A. Testbed

The mmWave testbed at 24 GHz ISM band used for our measurement is presented in Fig. 1. An existing vector network analyzer (VNA) from our lab was deployed to reduce the cost of the testbed. The VNA supports the frequency band from 100 kHz to 8.5 GHz. Therefore, the signal from the VNA must be up-converted at the transmitter and down-converted at the receiver. These additional RF circuitries required for the signal up and down-conversion, were bought from several

This work was partly supported by the European Commission within the European Regional Development Fund, through the Swedish Agency for Economic and Regional Growth, and partly by Region Gävleborg.

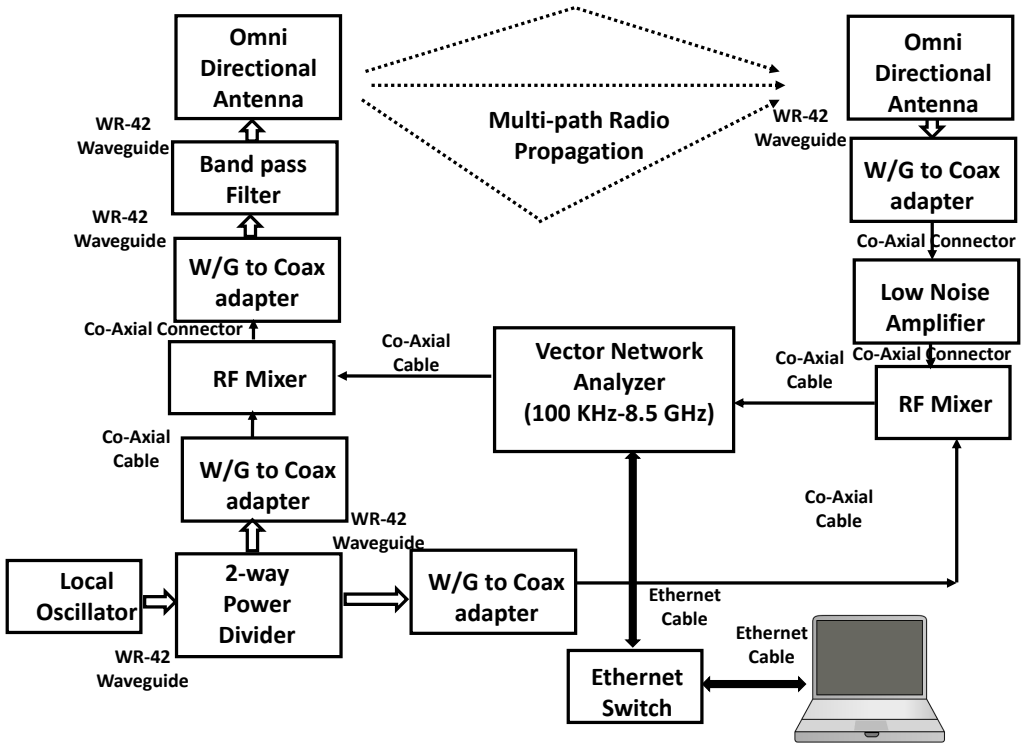

Fig. 1. Testbed for wideband channel characterization measurements

manufactures and assembled in our lab. Omni-directional antennas suitable for 24 GHz frequency band were chosen to be used both at the transmitter and receiver. The signal from a single local oscillator was used at both the mixers to achieve phase synchronization. The bandpass filter at the transmitter rejects the mirror frequencies, generated from the mixer. Additionally, a low noise amplifier was attached to the receiver antenna. An Ethernet switch was used to connect the VNA and the laptop, where an in-house developed Matlab programme controlled the VNA.

B. Measurement Environment

The measurements were carried out inside the robotics lab of the University of Gävle, Sweden. The approximate floor plan of the lab is shown in Fig. 2. The size of the lab is $12m \times 10m$. The ceiling of the lab is at the height of $3m$. The distance between the transmitter and receiver was kept $5m$. There are several glass partitions where robots are kept for user safety. There is a metallic cupboard inside the lab and a few metallic white-boards mounted on the walls. To summarize, this regular lab environment has more RF signal absorbing elements than the reflecting elements. Apart from the regular lab environment, we also carried out measurements in a reflective lab environment, where aluminium foils were stuck to the walls and other partitions at various strategic positions, in order to achieve more reflections.

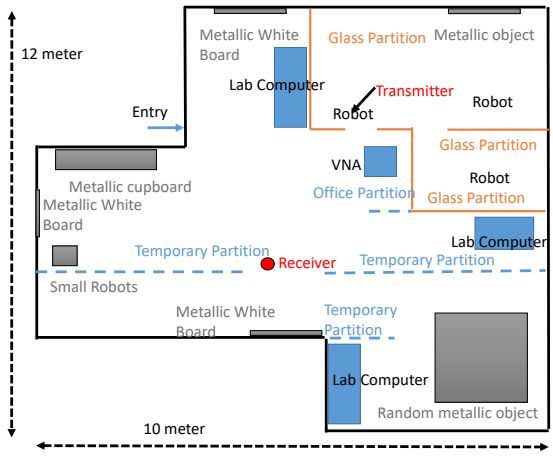

Fig. 2. Approximate floor plan of the Robotics lab, University of Gävle, Sweden.

C. Measurement Procedure

To create a motion in the test environment, the transmitter antenna was attached to the arm of a KUKA robot, as depicted in Fig. 3. The transmit antenna was roughly one meter above the ground. The deployed KUKA robot can attain a maximum speed of 2 m/s, which will generate a maximum Doppler shift of 160 Hz. The KUKA robot can be programmed to control the speed and direction of the movement. We measured

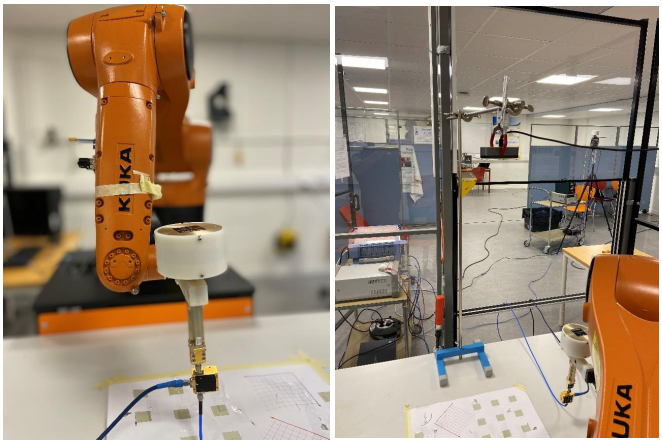

Fig. 3. Testbed at Robotics lab, University of Gävle, Sweden

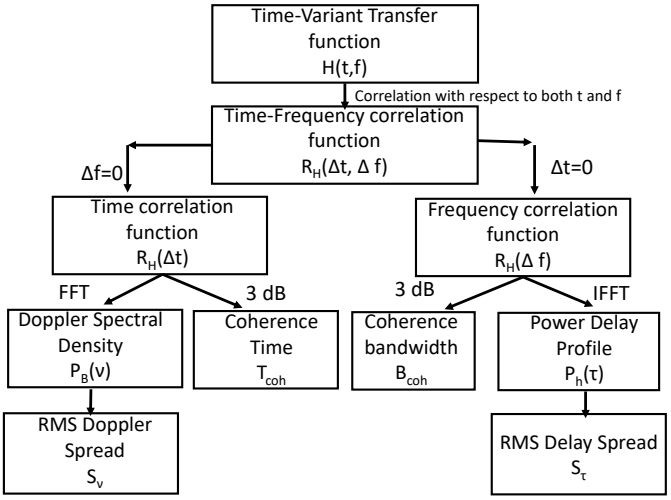

Fig. 4. Determination of various Wideband channel parameters. Motivated from Fig. 6.9 of [14].

the radio channel for two different velocities of the robot's arm, e.g., 2 m/s and 1 m/s. A '⊃' shaped movement was programmed in the vertical plane. The robot's arm was moved from left to right, moved down, and then moved to left. On the return journey, the robot's arm followed the reverse path. This movement was repeated several times for each experiment. The distance covered by the robot's arm from left to right, and from up and down movement was roughly 60 cm and 20 cm, respectively. Additionally, there was no movement programmed in the direction of the receiver. The receiving antenna was supported with the help of a tripod stand. The height of the receiving antenna can vary from 1.7 to 1.8 meters above the ground level. For each new measurement, the height of the antenna was increased 1 cm from the previous position. For a uniform scattering environment, the radio channel changes over distances of about half a wavelength. The half of a wavelength at 24 GHz frequency is 6.25 mm. Therefore, the receive antenna position was changed in steps of 1 cm to achieve different channel realization.

The wide-band channel characterization measurement was carried out over the entire ISM band, e.g., 250 MHz. The local oscillator was configured to oscillate at 22.125 GHz. The start and stop frequency in the VNA were set as 1.875 and 2.125 GHz, respectively. Therefore, the transmit antenna radiated in between 24 to 24.250 GHz. The number of measurement points configured in one sweep was 401, which helped to achieve a maximum detectable delay of 1600 ns; enough for an indoor environment. The Matlab program captured the $S21$ trace for all the frequency points, and it took roughly 8 msec on the average to complete one sweep in the frequency domain, including saving the trace data. $S21$ traces of 5000 complete sweeps were saved for a single receiver antenna height. Therefore, the maximum Doppler shift that can be detectable in this testbed is 125 Hz (ranging from -62.5 to 62.5 Hz).

First, a two-port Through–Open–Short–Match (TOSM) calibration was carried out without the antennas and the amplifier. Before removing the "Through" port, the amplifier was added at the receiver circuit, and the S21 traces were captured. The captured $S21$ traces of this stage were used to compensate the amplifier gain over different measured frequency points. Since the measured $S21$ traces were performed over a limited frequency band, there was a windowing effect on the results. Therefore, the measured $S21$ traces were weighted through a Blackman-Harris window [13] to reduce the windowing effect.

III. Wideband Channel Characterization

Fig. 4 presents the procedure to determine various wideband channel system functions and parameters from the time-variant transfer function when the Wide Sense Stationary and Uncorrelated Scatterers (WSSUS) conditions hold good [14]. The condition for WSSUS is typically fulfilled over an area of diameter about 10 times of the wavelength. Therefore, the experiment is planned by keeping the criteria for WSSUS into considerations. After weighing through a Blackman-Harris window [13], the captured S21 traces from the VNA provides the complex time-variant transfer function, $H(t, f)$ for a single receive antenna height. Here, f is one out of the 401 frequency points, and t is one out of the 5000 complete sweeps.

The time-frequency correlation function, $R_H(\Delta t, \Delta f)$ is the autocorrelation function of $H(t, f)$, e.g.,

$$R_H(t, t+\Delta t, f, f+\Delta f) = E\{H^*(t, f)\, H(t+\Delta t, f+\Delta f)\}, \quad (1)$$

where $[\bullet]^*$ is the conjugate transpose of a matrix and $\mathrm{E}[\bullet]$ is the expectation operator. As the WSSUS conditions hold good, $R_H(t, t+\Delta t, f, f+\Delta f) = R_H(\Delta t, \Delta f)$. The frequency correlation function, $R_H(\Delta f)$ can be obtained from the time-frequency correlation function by setting $\Delta t = 0$. Similarly, the time correlation function, $R_H(\Delta t)$ can be obtained from the time-frequency correlation function by setting $\Delta f = 0$.

The power delay profile (PDP), $P_h(\tau)$ in Fig. 4 gives the magnitude of a received signal as a function of time delay for a multi-path radio channel. It can be obtained from the

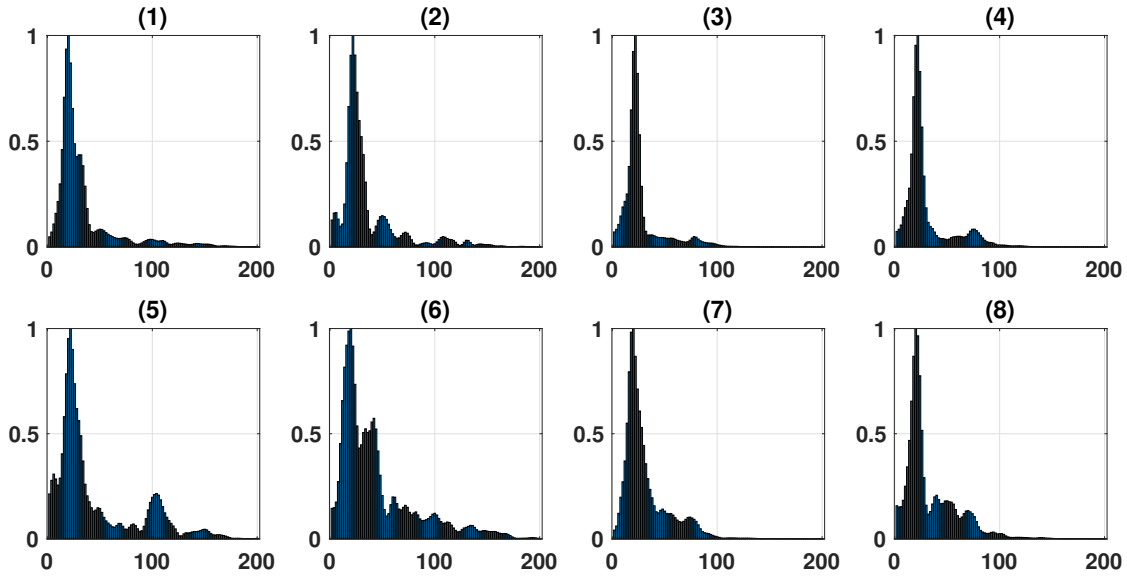

Fig. 5. Power Delay Profile plot at different circumstances. X-axis is delay in nano second. Y-axis is normalised power in linear scale. 1. LOS: High Speed Regular environment. 2. LOS: High Speed Reflective environment. 3. LOS: Low Speed Regular environment 4. LOS: Low Speed Reflective environment.5. NLOS: High Speed Regular environment. 6. NLOS: High Speed Reflective environment. 7. NLOS: Low Speed Regular environment 8. NLOS: Low Speed Reflective environment

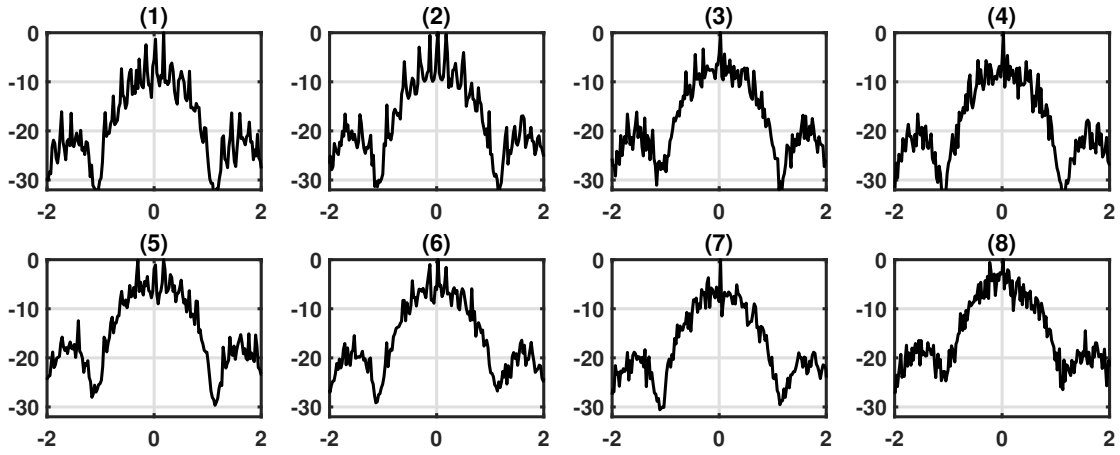

Fig. 6. Doppler spectral density plot at different circumstances. X-axis is doppler frequency in Hz. Y-axis is normalised power in dB scale. 1. LOS: High Speed Regular environment. 2. LOS: High Speed Reflective environment. 3. LOS: Low Speed Regular environment 4. LOS: Low Speed Reflective environment.5. NLOS: High Speed Regular environment. 6. NLOS: High Speed Reflective environment. 7. NLOS: Low Speed Regular environment 8. NLOS: Low Speed Reflective environment

frequency correlation function by the inverse fast Fourier transform (IFFT) operation. Moreover, the RMS delay spread is a widely used parameter of a multi-path radio channel and is determined from the PDP as [14]

$$S_\tau = \sqrt{\frac{\int_{-\infty}^{\infty} P_h(\tau)\tau^2 d\tau}{P_m} - T_m^2}, \tag{2}$$

where P_m is

$$P_m = \int_{-\infty}^{\infty} P_h(\tau) d\tau, \tag{3}$$

and T_m is

$$T_m = \frac{\int_{-\infty}^{\infty} P_h(\tau)\tau d\tau}{P_m}. \tag{4}$$

Similarly, the Doppler Spectral density (DSD), $P_B(\nu)$ in Fig. 4 gives the magnitude of a received signal as a function

of frequency shift due to relative movement in between transmitter and receiver. It can be obtained from the time correlation function by the fast Fourier transform (FFT) operation. Moreover, the RMS doppler spread is determined from the DSD as [14]

$$S_\nu = \sqrt{\frac{\int_{-\infty}^{\infty} P_B(\nu)\nu^2 d\nu}{P_{B,m}} - T_{B,m}^2}, \tag{5}$$

where $P_{B,m}$ is

$$P_{B,m} = \int_{-\infty}^{\infty} P_B(\nu) d\nu, \tag{6}$$

and $T_{B,m}$ is

$$T_{B,m} = \frac{\int_{-\infty}^{\infty} P_B(\nu)\nu d\nu}{P_{B,m}}. \tag{7}$$

As shown in Fig. 4, other important channel parameters are coherence bandwidth and coherence time. The coherence bandwidth is the range of frequencies over which the channel can be considered flat (3 dB). The coherence bandwidth is inversely proportional to the RMS delay spread. The coherence time is the duration of time over which the channel can be regarded as flat (3 dB). The coherence time is inversely proportional to the RMS doppler spread.

IV. Measurement Results and Analysis

Fig. 5 and 6 in the previous page depict the power delay profile and Doppler spectral density at various situations, respectively. Fig. 7 presents a comparison of the RMS delay spread and coherence bandwidth for different experimental situations and receiver antenna heights. Additionally, Fig. 8 presents a comparison of the RMS Doppler Spread and coherence time. In these figures, the scenarios of a reflective

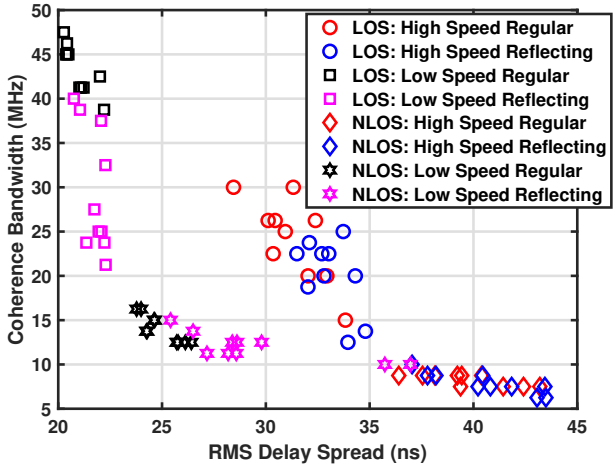

Fig. 7. RMS Delay Spread and Coherence Bandwidth at different situations for different experimental situations and receiver antenna heights.

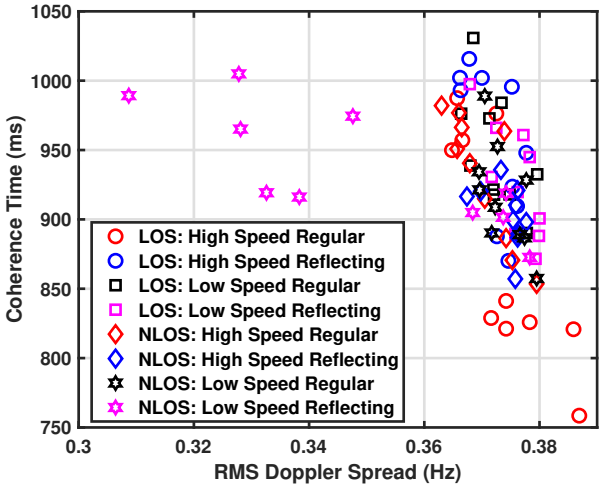

Fig. 8. RMS Doppler Spread and Coherence Time at different situations for different experimental situations and receiver antenna heights.

environment were achieved by sticking the aluminium foils to the walls and other partitions at various strategic locations. The NLOS situation was created by placing a temporary partition block in between the transmitter and receiver. In Fig. 3, some of the blue coloured temporary partition blocks can be visible. Additionally, we measured the radio channel for two different speed of the robot's arm, e.g., 2 m/s and 1 m/s.

From Fig. 5, the following conclusions are derived. A greater number of multipath components are observed in the NLOS situations. Between reflective and regular environments, more number of multipath components are visible in reflective environments. Additionally, high-speed situations observe more number of multipath components than its low-speed counterpart. To further investigate the effect of reflections of the radio waves, the RMS delay spread and coherence bandwidth is estimated and presented in Fig. 7. According to the theory, the RMS delay spread is inversely proportional to the coherence bandwidth. For example, in a situation, where a large number of multipath components are observed, the RMS delay spread is higher, and the coherence bandwidth is lower. However, it can be seen in Fig. 7 that there is no unique proportion that applies to all the relationship. In Fig. 7, it can be observed that the LOS low-speed situations have a lower RMS delay spread and a higher coherence bandwidth than the NLOS low-speed situations. Similarly, the LOS high-speed situations have a lower RMS delay spread and a higher coherence bandwidth than the NLOS high-speed situations. However, the NLOS low-speed situations have a lower RMS delay spread and a lower coherence bandwidth than the LOS high-speed situations. Additionally, for the same scenarios, the relationship between RMS delay spread and the coherence bandwidth changes for different receiver antenna height. Therefore, it is found that the environmental aspects also play important roles in the power delay profile, for example, how the reflections from different clusters reach the

receiver.

From Fig. 6, we can observe significant Doppler shift, mostly centered around the zeroth frequency. The smaller RMS Doppler spread seen in Fig. 8 further confirms this observation. The RMS Doppler spread is inversely proportional to the coherence time. However, like the previous result, there is no unique proportion that applies to all the relationship. It can be seen that the relationship between RMS Doppler spread and the coherence time changes for different receiver antenna height of the same scenarios. Therefore, it is found that the environmental aspects also play important roles in the Doppler spectral density. In our experiment, we did not observe very large Doppler shift. This could be due to both experimental and environmental factors. The Robotics lab of the University of Gävle has very few RF signal reflecting elements, even after additional reflection is achieved artificially. Additionally, the loss due to reflection is high at 24 GHz. The distance between the transmitter and receiver was kept 5 meters. The distance covered by the robot's arm from left to right, and from up and down movement was roughly 60 cm and 20 cm, respectively. Additionally, there was no movement programmed in the direction of the receiver. Therefore, the angle between the direction of the robot's arm movement and the line of sight from the transmitter to the receiver is mostly close to 90 degree, e.g., roughly 90 ± 3 degrees.

V. Conclusion

In this research work, we investigate the wide-band channel characteristics at 24 GHz ISM band in a mobile radio environment. The mobility in the test environment is achieved by attaching the transmit antenna to a KUKA robot's arm. The radio channel measurements were carried out inside the robotics lab at the University of Gävle, Sweden. Here, we investigated the multi-path and the Doppler effect and quantified them with the help of the wide-band channel parameters, like RMS delay spread, RMS Doppler spread, coherence bandwidth and coherence time. In our investigation, we found that the maximum number of multi-path components are visible in an NLOS reflective environment with high velocity. In contrast, the minimum number of multi-path components are visible in a LOS regular environment with a lower velocity. In our experiment, the Doppler shift is mostly observed close to the zeroth frequency, as the robot's arm movement direction is close to perpendicular to the LOS from the transmitter to the receiver. Additionally, the environmental aspects play important roles in deciding the relationship between RMS Delay spread and coherence bandwidth, or between RMS Doppler spread and coherence time.

References

[1] A. Osseiran, F. Boccardi, V. Braun, K. Kusume, P. Marsch, M. Maternia, O. Queseth, M. Schellmann, H. Schotten, H. Taoka, H. Tullberg, M. A. Uusitalo, B. Timus, and M. Fallgren, "Scenarios for 5G mobile and wireless communications: the vision of the METIS project," *IEEE Communications Magazine*, vol. 52, no. 5, pp. 26–35, may 2014.

[2] E. Violette, R. Espeland, R. DeBolt, and F. Schwering, "Millimeter-wave propagation at street level in an urban environment," *IEEE Transactions on Geoscience and Remote Sensing*, vol. 26, no. 3, pp. 368–380, may 1988.

[3] S. Sun, T. A. Thomas, T. S. Rappaport, H. Nguyen, I. Z. Kovacs, and I. Rodriguez, "Path Loss, Shadow Fading, and Line-of-Sight Probability Models for 5G Urban Macro-Cellular Scenarios," in *2015 IEEE Globecom Workshops (GC Wkshps)*. IEEE, dec 2015, pp. 1–7.

[4] T. S. Rappaport, G. R. MacCartney, M. K. Samimi, and S. Sun, "Wideband Millimeter-Wave Propagation Measurements and Channel Models for Future Wireless Communication System Design," *IEEE Transactions on Communications*, vol. 63, no. 9, pp. 3029–3056, sep 2015.

[5] S. Deng, M. K. Samimi, and T. S. Rappaport, "28 GHz and 73 GHz millimeter-wave indoor propagation measurements and path loss models," in *2015 IEEE International Conference on Communication Workshop (ICCW)*. IEEE, jun 2015, pp. 1244–1250.

[6] G. R. MacCartney, T. S. Rappaport, S. Sun, and S. Deng, "Indoor office wideband millimeter-wave propagation measurements and channel models at 28 and 73 GHz for Ultra-Dense 5G Wireless Networks," *IEEE Access*, vol. 3, pp. 2388–2424, 2015.

[7] B. Ai, K. Guan, R. He, J. Li, G. Li, D. He, Z. Zhong, and K. M. S. Huq, "On Indoor Millimeter Wave Massive MIMO Channels: Measurement and Simulation," *IEEE Journal on Selected Areas in Communications*, vol. 35, no. 7, pp. 1678–1690, 2017.

[8] O. H. Koymen, A. Partyka, S. Subramanian, and J. Li, "Indoor mm-Wave Channel Measurements: Comparative Study of 2.9 GHz and 29 GHz," in *2015 IEEE Global Communications Conference (GLOBECOM)*. IEEE, dec 2014, pp. 1–6.

[9] X. Wu, C. X. Wang, J. Sun, J. Huang, R. Feng, Y. Yang, and X. Ge, "60-GHz Millimeter-Wave Channel Measurements and Modeling for Indoor Office Environments," *IEEE Transactions on Antennas and Propagation*, vol. 65, no. 4, pp. 1912–1924, 2017.

[10] S. Piersanti, L. A. Annoni, and D. Cassioli, "Millimeter waves channel measurements and path loss models," in *2012 IEEE International Conference on Communications (ICC)*. IEEE, jun 2012, pp. 4552–4556.

[11] S. Geng, J. Kivinen, X. Zhao, and P. Vainikainen, "Millimeter-wave propagation channel characterization for short-range wireless communications," *IEEE Transactions on Vehicular Technology*, vol. 58, no. 1, pp. 3–13, 2009.

[12] J. Senic, C. Gentile, P. B. Papazian, K. A. Remley, and J. K. Choi, "Analysis of E-Band Path Loss and Propagation Mechanisms in the Indoor Environment," *IEEE Transactions on Antennas and Propagation*, vol. 65, no. 12, pp. 6562–6573, 2017.

[13] M. S. Varela and M. G. Sánchez, "RMS delay and coherence bandwidth measurements in indoor radio channels in the UHF band," *IEEE Transactions on Vehicular Technology*, vol. 50, no. 2, pp. 515–525, 2001.

[14] A. F. Molisch, *WIRELESS COMMUNICATIONS*. John Wiley & Sons, 2012.